

The Initial-Final Mass Relation among White Dwarfs in Wide Binaries

J. K. Zhao^{1,2}, T. D. Oswalt¹, L. A. Willson³, Q. Wang³, G. Zhao²

ABSTRACT

We present the initial-final mass relation derived from 10 white dwarfs in wide binaries that consist of a main sequence star and a white dwarf. The temperature and gravity of each white dwarf was measured by fitting theoretical model atmospheres to the observed spectrum using a χ^2 fitting algorithm. The cooling time and mass was obtained using theoretical cooling tracks. The total age of each binary was estimated from the chromospheric activity of its main sequence component to an uncertainty of about 0.17 dex in $\log t$. The difference between the total age and white dwarf cooling time is taken as the main sequence lifetime of each white dwarf. The initial mass of each white dwarf was then determined using stellar evolution tracks with a corresponding metallicity derived from spectra of their main sequence companions, thus yielding the initial-final mass relation. Most of the initial masses of the white dwarf components are between 1 - 2 M_{\odot} . Our results suggest a correlation between the metallicity of a white dwarf's progenitor and the amount of post-main-sequence mass loss it experiences - at least among progenitors with masses in the range of 1 - 2 M_{\odot} . A comparison of our observations to theoretical models suggests that low mass stars preferentially lose mass on the red giant branch.

Subject headings: white dwarfs: Stars — Activity: Stars

1. Introduction

Over 90 percent of all stars shed at least half their mass as they evolve towards their final state - a white dwarf (WD). The initial-final mass relation (IFMR) represents a mapping

¹Florida Institute of Technology, Melbourne, USA, 32901; jzhao@fit.edu; toswalt@fit.edu

²Key Laboratory of Optical Astronomy, National Astronomical Observatories, Chinese Academy of Sciences, Beijing, 100012, China; gzhaob@bao.ac.cn

³Department of Physics and Astronomy, Iowa State University, Ames, IA 50010, USA; lwillson@iastate.edu; wqinisu@iastate.edu

between the mass of a WD remnant and the mass of its hydrogen-burning main-sequence (MS) progenitor. It also characterizes the amount of material stars with primordial masses $M \lesssim 8 M_{\odot}$ recycle to the interstellar medium. Thus, it is of paramount importance to understanding the chemical enrichment and the efficiency of star formation in galaxies. This relation is also a key constraint on stellar evolution theory.

One of the first attempts to empirically determine the IFMR was undertaken by Weidemann (1977). Reimers & Koester (1982) and Koester & Reimers (1996) presented observations of WDs in the open cluster NGC 2516 and obtained an IFMR using these WDs. Weidemann (2000; W00 hereafter) updated the IFMR by incorporating new theoretical and observational data. Claver et al. (2001) observed six WDs in the Praesepe open cluster and determined a monotonic IFMR. Williams et al. (2004; 2009) presented an empirical determination of the IFMR based on a spectroscopic analysis of massive white dwarfs in NGC 2168 (M35). They showed that the resultant white dwarf mass increases monotonically with progenitor mass for masses greater than $4 M_{\odot}$. Ferrario et al. (2005) re-evaluated the ensemble of data that has been used to determine the IFMR and characterized a mean IFMR about which there is an intrinsic scatter. They showed that a linear IFMR predicts a mass distribution in reasonable agreement with the Palomar-Green survey. Kalirai et al. (2005) determined the IFMR from observations of very faint WDs in the rich open cluster NGC2099 (M37). They found stars with initial masses between 2.8 and $3.4 M_{\odot}$ lose 70 - 75% of their mass during post-MS evolution. Dobbie et al. (2006) also constructed a new IFMR based on 11 WDs in the Praesepe open cluster. Rubin et al. (2008) constructed an IFMR based on 19 spectroscopically identified WDs in NGC 1039 (M34). Catalán et al. (2008a) studied the IFMR using six WDs in wide binaries and suggested the IFMR may not be a single-valued function. Kalirai et al. (2008) presented constraints on the low-mass end of the IFMR using older open clusters NGC7789 ($t = 1.4$ Gyr), NGC 6819 ($t = 2.5$ Gyr) and NGC6791 ($t = 8.6$ Gyr). Later, Kalirai et al. (2009) extended the IFMR to lower masses using the globular cluster M4. Since most nearby clusters are relatively young, the initial masses of those WDs tend to be high.

In this paper we investigate the IFMR using wide “fragile” binary systems containing a WD with a MS companion. The systems have relatively large orbital separations ($< a > \sim 10^3$ AU; Oswalt et al. 1993; Silvestri et al. 2001, 2002, 2005). Thus, one can safely assume that each component has evolved independently, unaffected by mass exchange or tidal coupling that complicate the evolution of closer pairs. Components of a given binary are coeval (Greenstein 1986). Essentially, each may be regarded as an open cluster with only two components. Although it is difficult to obtain ages for wide binaries as accurate as ages for open clusters, they tend to be nearer, brighter and are far more numerous than nearby clusters. Moreover, they span a much more continuous range in age. Catalán et al. (2008a;

C08a hereafter) used six wide binaries to investigate the IFMR; three of the WDs had low initial mass ($< 2M_{\odot}$). Our sample contains additional WDs at the low initial mass limit.

Previous research has indicated a large scatter in the empirical IFMR. What is the source of this scatter? Kalirai et al. (2005) found some weak evidence of a metallicity dependence in the IFMR. Kalirai et al. (2007) found evidence for enhanced mass loss at extremely high metallicities by studying the white-dwarf mass distribution in the supersolar-metallicity star cluster NGC 6791 ($[\text{Fe}/\text{H}] = +0.4$). Kalirai et al. (2009) found a relatively flat relation between mass loss and metallicity ($[\text{Fe}/\text{H}]$ between -1.1 to solar metallicity) by extending these studies to WDs in the globular cluster M4. However, a clear relation between the metallicity and scatter in the IFMR has not been demonstrated (cf. Williams 2007; Catalán et al. 2008b, C08b hereafter). We investigated whether there is a metallicity dependence on the IFMR in our wide binary sample using the spectra of their MS companions.

Section 2 provides an overview of the observations and reductions for our sample. The astrophysical properties of the WDs are discussed in section 3. The MS companions are discussed in section 4. In section 5, we present and discuss our IFMR. Section 6 compares our observations to theoretical models of post-MS mass loss. A discussion of the implications of our findings is given in section 7.

2. Observations and Data Reduction

Most of the MS+WD binaries chosen for this study are from the Luyten (1979) and Giclas, Burnham & Thomas (1971) proper motion catalogs chosen by Oswalt, Hintzen & Luyten (1988). A key impetus for using such pairs for determining the IFMR is that the total lifetime of each pair is approximately the age derived from measurements of the MS component. In addition, the total age of a pair is approximately the sum of each WD component’s cooling time and the MS lifetime of its progenitor.

Table 1 gives our observed data for 11 wide binaries. Columns 1-3 list the name of each binary, its right ascension, and declination (coordinates are the original 1950 catalog epoch). Columns 4-5 present the ID and spectral type of each WD component. Columns 6-7 list the spectroscopic observation date and site.

2.1. Spectroscopic Observations

Spectroscopic observations were made at two observatories. In the southern hemisphere, observations were conducted at Cerro Tololo Inter-American Observatory (CTIO) using the

Blanco 4-meter telescope. Northern hemisphere observations were conducted at Kitt Peak National Observatory (KPNO) using the Mayall 4-meter telescope.

At CTIO, the Ritchey-Chretien (RC) Cassegrain spectrograph on the 4-meter Blanco telescope was used on two separate observing runs (February 2004 and February 2005) to obtain optical spectroscopy of wide pairs, as well as standard flux calibration stars. During these two observing runs the KPGL1 grating was used to obtain a scale of $0.95 \text{ \AA}/\text{pixel}$ ($R \sim 2000$). A Loral 3K CCD (L3K) was used with the RC spectrograph. It is a thinned $3K \times 1K$ CCD with $15 \mu\text{m}$ pixels. A spectral range of approximately $3800 - 6700 \text{ \AA}$ was achieved.

At KPNO, the RC spectrograph with the BL450 grating set for the 2nd order to yield a resolution of $0.70 \text{ \AA}/\text{pixel}$ ($R \sim 2000$) was used to obtain optical spectra during November 2006 and July 2010 with the Mayall 4-meter telescope. The $2K \times 2K$ T2KB CCD camera with $24 \mu\text{m}$ pixels was used to image the spectra. An 8-mm CuSO_4 order-blocking filter was added to decrease 1st-order overlap at the blue end of the spectrum. A spectral range of approximately $3800 - 5000 \text{ \AA}$ was achieved.

2.2. Data Reduction

The data were reduced with standard IRAF¹ reduction procedures. In all cases, program objects were reduced with calibration data (bias, flat, arc, flux standard) taken on the same night. Data were bias-subtracted and flat-fielded, and one-dimensional spectra were extracted using the standard aperture extraction method. A wavelength scale was determined for each target spectrum (including stellar flux standards) using HeNeAr arc lamp calibrations. Flux standard stars were used to place the spectra on a calibrated flux scale. We emphasize that the final flux calibrations for the targets provide only relative fluxes, as most nights were not spectrophotometric.

The radial velocity of each MS star was determined by cross-correlation between the observed spectra and a set of MS template spectra. The F, G and K template spectra were generated from a theoretical atmosphere grid (Castelli & Kurucz 2003). The dM template spectra were compiled using observed M dwarf spectra from the Sloan Digital Sky Survey (SDSS)². The wavelength ranged from roughly $3900 - 9200 \text{ \AA}$ (see Bochanski et al. 2007).

¹IRAF is distributed by the National Optical Astronomy observatories, which are operated by the Association of Universities for Research in Astronomy, Inc., under cooperative agreement with the National Science Foundation (<http://iraf.noao.edu>).

²<http://www.astro.washington.edu/slh/templates>

Our typical internal measurement uncertainties in radial velocity were $\sigma_{v_r} = \pm 4.6 \text{ km s}^{-1}$.

3. Analysis of White dwarfs

3.1. Determination of T_{eff} and $\log g$

Our sample included nine DA WDs and two DB WDs. For DA WDs the T_{eff} and $\log g$ were derived via simultaneous fitting of the H β to H8 Balmer line profiles using the procedure outlined by Bergeron et al. (1992). The line profiles in both observed spectra and model spectra were first normalized using two points at the continuum level on either side of each absorption line. Thus, the fit should not be affected by the flux calibration. Model atmospheres used for this fitting were derived from model grids provided by Koester (2010). Details of the input physics and methods can be found in that reference. Fitting of the line profiles was carried out using the IDL package MPFIT (Markwardt 2008), which is based on χ^2 minimization using the Levenberg-Marquardt method. This package can be downloaded from the project website³. Errors in the T_{eff} and $\log g$ were calculated by stepping the parameter in question away from their optimum values and redetermining minimum χ^2 until the difference between this and the true minimum χ^2 corresponded to 1σ for a given number of free model parameters. Our spectra of the DB WDs were not of high enough signal-to-noise ratio (S/N) to do line profile fitting on such weak lines. For these DB WDs we adopted the T_{eff} and $\log g$ from Voss et al. (2007).

Fig. 1 shows fits of the observed Balmer lines of the nine DA WDs. The derived T_{eff} , $\log g$ and uncertainties are shown in columns 2-3 of Table 2. Estimated T_{eff} and $\log g$ for nine DAs were also available in the literature, allowing the comparisons shown in Fig. 2. For most of the WDs, the difference between our T_{eff} value and the literature value is smaller than 1000 K and the $\log g$ difference is smaller than 0.1 dex. For WD1544-374, our $\log g$ is consistent with that of C08a and Kawka et al. (2007) but differs by 0.2 dex with that of Vauclair et al. (1997). For WD2253-08, the $\log g$ values in the literature differ substantially, however, our value is consistent with that of C08a. In Fig. 2, the dotted line represents the unit slope relation. In general, our results are consistent with those in the literature.

Reid (1996) reported that the pair BD+44 1847/G116-16 is a non-physical pair because the gravitational redshift $K_{\text{RS}} = 113.9 \text{ km s}^{-1}$ corresponds to $1.1 M_{\odot}$ which is inconsistent with $0.75 M_{\odot}$ from line profile fitting by Bergeron et al. (1995). We determined a mass of $0.77 M_{\odot}$ that is almost the same as Bergeron et al. (1995). Although our spectral resolution is

³<http://purl.com/net/mpfit>

only $\sim 1.8 \text{ \AA}$, we attempted a rough redshift measurement of this pair. The doppler shift of the WD component measured from $H\beta$ was about $120 \pm 10 \text{ km s}^{-1}$ which is consistent with that of Reid (1996). The parallaxes of the components from Simbad Astronomical Database (Genova 2006) for this pair are 34.6 mas and 19.36 mas for the primary and secondary, respectively. Hence, we also conclude this pair is non-physical. It was therefore eliminated from our determination of the IFMR.

3.2. Determination of WD cooling times and mass

From our T_{eff} and $\log g$ estimation for each star, its current mass (M_f) and cooling time (t_{cool}) were estimated from Bergeron’s cooling sequences⁴. For the pure hydrogen model atmospheres hotter than $T_{\text{eff}} = 30,000 \text{ K}$, we used the carbon-core cooling models of Wood (1995), with thick hydrogen layers of $q_H = M_H/M_* = 10^{-4}$. For T_{eff} cooler than 30, 000 K we used cooling models similar to those described in Fontaine et al. (2001) but with carbon-oxygen cores and $q_H = 10^{-4}$ (see Bergeron, Leggett & Ruiz 2001). For the pure helium atmospheres we used similar models but with $q_H = 10^{-10}$. M_{WD} and t_{cool} were then calculated by spline interpolation based on the T_{eff} and $\log g$. The final M_{WD} and t_{cool} values are shown in columns 4-5 of Table 2. The uncertainties in mass are estimated based on the uncertainties in T_{eff} and $\log g$ when interpolating in the cooling sequences. The average mass of our 11 WDs is $0.628 M_{\odot}$. The average mass of only the 9 DA WDs is $0.635 M_{\odot}$, which is consistent with Bergeron et al. (1995; $0.626 M_{\odot}$).

4. Analysis of the Main Sequence Stars

The components of each wide binary share the same original properties such as age, chemical composition and dynamics (Greenstein 1986). Thus, the MS components of wide binaries provide valuable information about the progenitors of their WD companions.

4.1. The age determination

Age is one of the most difficult to determine properties of any star. Ages for single lower MS stars derived from isochrone fitting are especially uncertain because of the narrow vertical dispersion of isochrones within the MS in an H-R diagram. Small uncertainties in

⁴The cooling sequences can be downloaded from the website: <http://www.astro.umontreal.ca/~bergeron/CoolingModels/>.

luminosity and metallicity propagate into large uncertainties in age. Lachaume et al. (1999) investigated the precision of age determinations for a sample of nearby MS stars of spectral types B9-K9. They found the isochrone method is best for hot stars, while stellar rotation (Barnes 2007) is best for cool stars. The MS components of our wide binaries are F-K stars. Most of our wide binaries are older than 1 Gyr, so measurement of their rotation period would require a large investment of observing time and very precise photometry.

For decades, chromospheric activity (CA) has been known to inversely correlate with stellar age (Skumanich 1972). Early work by Wilson (1963; 1968) and Vaughan & Preston (1980) established CaII H&K emission as a useful marker of CA in lower MS stars. The most commonly used measurement index of CaII H&K emission is R'_{HK} , defined as the ratio of the emission from the chromosphere in the cores of the CaII H&K lines to the total bolometric emission of the star. Soderblom et al. (1991), Lachaume et al. (1999) and Mamajek & Hillenbrand (2008) presented detailed investigations of the relation between R'_{HK} and stellar age.

Soderblom et al. (2010; Fig. 8) compared ages of G dwarfs derived from isochrone placement and from HK activity index. It is clear that the isochrone ages were larger than activity ages. For some stars, isochrone ages were inconsistent with the age of Galactic disk. Most stars in our sample are late main sequence G stars and K stars, for which the isochrone method does not work well, as discussed above.

Following Hall et al. (2007), for each star we computed the flux ratio S_{HK} :

$$S_{\text{HK}} \equiv \alpha \frac{\text{H} + \text{K}}{\text{R} + \text{V}} \quad (1)$$

where H and K are the fluxes measured in 2 \AA rectangular windows centered on the line cores of CaII H&K; R and V are the fluxes measured in 20 \AA rectangular ‘pseudocontinuum’ windows on either side. These bands are similar to those used in the Mount Wilson chromospheric activity survey program (Baliunas et al. 1995), except that the bands centered on Ca II H&K are wider (2 \AA) than those used at Mount Wilson (1 \AA) because of our instrumental resolution. Here α is 10, indicating the pseudocontinuum windows are 10 times wider than the H&K windows in wavelength coverage. Fig. 3 presents our H&K measurements for these 10 MS stars.

In order to derive a transformation relation between our instrumental systems and the Mount Wilson system we selected six stars which have stable CA from Baliunas et al. (1995) as ‘standard CA stars’. Since S_{MW} values for four MS stars in our CTIO sample were found in the literature, we only observed these ‘CA standard stars’ with KPNO telescope. Table 3 provides data for these standard stars. Column 1 lists the stars’ name; columns 2 - 3 give

our S_{HK} and the published S_{MW} respectively. Fig. 4 shows the correlation between S_{HK} and published S_{MW} ; Equation 2 is the transformation equation obtained by a least squares fit. The scatter is $\sigma_{S_{\text{MW}}} = 0.017$.

$$S_{\text{MW}} = -0.069 + 1.308S_{\text{HK}} \quad (2)$$

The range of S_{HK} for which Equation 2 applies is limited by the range of S_{HK} in ‘standard CA stars’, which is about $0.15 < S_{\text{HK}} < 0.55$. With Equation 2, the S_{HK} value we measured at KPNO can be directly transformed to S_{MW} . For wide binary stars observed at CTIO we adopted the S_{MW} values from the literature wherever possible. If more than one value was available in the literature, reference was given to those derived from higher resolution spectra. This is based on the conclusion by Jenkins et al. (2011) that CA measures from low resolution spectra significantly increase the rms scatter when calibrating onto a common system such as the Mt. Wilson system. The S_{MW} values of CD-59 1275 and CD-38 10983 were obtained from Henry et al. (1996); 40 Eri A came from Baliunas et al. (1995) and CD-37 10500 was found in Jenkins et al. (2011). Only two MS stars observed at CTIO did not have S_{MW} values in the literature. For these, the S_{HK} (CTIO) were first calibrated into S_{HK} (KPNO) using the empirical relation between the two instrument (Zhao et al. 2011a): $S_{\text{HK}} (\text{CTIO}) = S_{\text{HK}} (\text{KPNO}) + 0.095$. Then, the S_{MW} of these two stars were computed using Equation 2. For the wide binary MS stars observed at KPNO, the S_{MW} were directly calculated from Equation 2.

The S_{MW} index includes both photospheric and chromospheric contributions. The photospheric flux can be removed approximately using the procedure of Noyes et al. (1984), who derived a quantity $R_{\text{HK}} \propto F_{\text{HK}}/\sigma T_{\text{eff}}^4$, where F_{HK} is the flux per square centimeter in the H and K band passes. The quantity R_{HK} can be derived from S_{MW} by modeling the variation in the continuum fluxes as a function of effective temperature (using B-V as a proxy). R_{HK} must then be further corrected by subtracting the photospheric contribution in the cores of the H and K lines. The logarithm of the final quantity R'_{HK} is a useful measure of the chromospheric emission, essentially independent of the effective temperature.

We computed R'_{HK} for the six stars observed at CTIO and the five stars observed at KPNO. Their colors (B-V) meet the condition of Noyes et al. (1984; B-V < 1.1). Both the estimates of S_{MW} and $\log R'_{\text{HK}}$ are tabulated for our program stars in Table 4.

CA vs. age relations were published by Soderblom et al. (1991); Donahue (1998); Lachaume et al. (1999) and Mamajek & Hillenbrand (2008). Rocha-Pinto & Maciel (1998) investigated the metallicity dependence of the Soderblom et al. (1991) relation. Because we

intended to explore the effects of metallicities within our sample, we used their relation to estimate our ages.

$$\log t = (-1.50 \pm 0.003)\log R'_{\text{HK}} + (2.25 \pm 0.12) \quad (3)$$

$$\Delta\log t = -0.193 - 1.382[\text{Fe}/\text{H}] - 0.213[\text{Fe}/\text{H}]^2 + 0.270[\text{Fe}/\text{H}]^3 \quad (4)$$

The total age estimates and uncertainties for our program stars derived from Equations 3 - 4 are listed in column 6 of Table 4. The age uncertainties originate mainly from the S_{HK} uncertainties as they affect Equation 3. The S_{HK} uncertainties are determined from the average of the standard deviations of measurements for stars with more than two observations (about $\pm 4.6\%$). The total internal uncertainty of our age determinations is about ± 0.17 dex. Independent age determinations for a couple of pairs were found in the literature. These pairs are listed in Table 5. Column 1 gives their identifications. Columns 2, 3 and 4 list the ages included in Holmberg et al. (2009), Valenti & Fischer (2005) and Barnes (2007), respectively. Our ages are younger than isochrone fitting ages in all four cases. For 40 Eri A, the isochrone fitting age is unreasonably large, while our age for this star is close to the rotation age 4.75 ± 0.75 Gyr from Barnes (2007). For CD-38 10983, our age is also consistent with the rotation age, but younger than the isochrone age, which has a large uncertainty. For CD-59 1275, our age is close to the isochrone age. For CD-37 10500, the error bar is too large for the isochrone age to be useful. Thus, even in this small sample it can be seen how difficult it is to get consistent isochrone ages for late G and K dwarfs. Small uncertainties in luminosity and metallicity cause large uncertainties in age.

Ages from isochrone fitting of clusters with well defined turnoffs are unquestionably more accurate than those of single field stars. To estimate the accuracy of our CA age estimates, we selected 75 member stars in M67 having R'_{HK} and B-V data from Mamajek & Hillenbrand (2008). All the original HK observations of these objects are from Giampapa et al. (2006). The CA age of each member star was estimated with the above formula. Fig. 5 is the resulting CA age distribution of this sample. The dotted line is a Gaussian fit. The average age of those member stars is 3.28 Gyr with 1σ 0.95 Gyr (1-sigma uncertainty of 29%). The difference between the average CA age for this cluster and its turnoff age (4.0 Gyr) is about 0.73 Gyr. This difference, about 18%, is well within the formal uncertainties of our wide binaries' age determinations.

All are M67 stars discussed above are solar-type dwarfs, which are likely to have activity cycles, perhaps similar to the Sun's 11-22 year period. The stars with very high HK values

could have been observed at maximum activity during their cycle (perhaps a few are close interacting binaries). The stars with very low HK values could be in a Maunder minimum state. Most likely these are the main sources of scatter in CA ages derived from coeval populations of stars like clusters. We did not attempt to quantify these factors here because each of our objects has so far only been observed a small number of times. This is almost certainly the dominant source of scatter in CA ages.

As a final reality check, we randomly drew 10 stars from the data shown in Fig. 5 and computed the age and 1σ estimates. The age of M67 derived from a 10-star sample is $3.3 \text{ Gyr} \pm 0.9$, which represents a 28% uncertainty—very comparable to the 30% claimed by Soderblom (2010) and others for CA age determinations. In our 10 wide binary sample the formal age uncertainty is 0.17 dex (48%; computed from uncertainties listed Table 1). We do not propose that the age of any single star has been determined to a precision any better than this. These uncertainties have been fully propagated into the error bars shown in the plots shown in Figs. 6 and 7 below.

The difference between the total age of a MS star and the cooling age of its WD companion provides an estimate of the latter’s progenitor MS lifetime (given in column 6 of Table 2).

4.2. The metallicity measurements

The metallicity of each MS star was measured by comparing the observed spectrum to a set of template spectra. Initially, a library of low resolution theoretical spectra was generated using the SYNTH program based on Kurucz’s New Opacity Distribution Function atmospheric models (Castelli & Kurucz 2003). The details can be found in Zhao et al. (2011a, b). Fig. 3 of Zhao et al. (2011a) presents an example of how we determined stellar metallicity and its uncertainty in 40 Eri A. The final $[\text{Fe}/\text{H}]$ values are given in column 7 of Table 2. In Sec. 6, the metallicity is indicated by Z , where $[\text{Fe}/\text{H}] = 0.0$ is equivalent to $Z = 0.019$.

5. Initial-final mass relation

Once the MS lifetimes of the WDs and the metallicities of their companions were obtained, the WD initial masses were estimated from evolution models (Girardi et al. 2000) by interpolation among the tables for $Z = 0.030, 0.019, 0.008$ and 0.004 . The initial (M_i) and final masses (M_f) obtained are listed in columns 8 and 4 of Table 2, respectively.

Fig. 6 displays the resulting empirical IFMR obtained for 10 WDs in our sample (filled circles). Diamonds represent the WDs in wide binaries from C08a. Our sample has three pairs in common with C08a: 40 Eri A/B, CD-38 10980/CD-30 10983 and L481-60/CD-37 10500. The solid lines in Fig. 6 connect our values to those of C08a. For L481-60/CD-37 10500, both M_i and M_f are consistent with those in C08a. However, our M_i is different for WDs in the other two pairs. In C08a, the total ages of the binaries were estimated from the X-ray fluxes of their MS components, while our ages are from the S_{HK} of the MS stars. For 40 EriA (HD26965), C08a gives an age of 1.07 Gyr. Our age is 3.56 Gyr, which is closer to its rotation age (4.7 Gyr; Barnes 2007). For CD-38 10983 (HD147513), C08a gives an age of 0.33 Gyr. Our age is 0.55 Gyr, which is also more consistent with the rotation age 0.58 Gyr (Barnes 2007). Moreover, the ages of our 10 pairs are all from the same CA vs. age relation, so no scatter due to the different methods of age determination is imposed.

As can be seen in Table 4, our wide binaries range in age from 0.55 Gyr to 6.54 Gyr. M_i ranges from $1.11 M_{\odot}$ to $4.14 M_{\odot}$. $[\text{Fe}/\text{H}]$ ranges from -0.40 to $+0.19$ dex. Six WDs have M_i lower than $2.0 M_{\odot}$. Thus, wide binaries provide very promising leverage for investigations of the IFMR at masses that are difficult to reach in clusters.

The dotted line in Fig. 6 indicates the semi-empirical IFMR from W00. The dash-dot line is the semi-empirical IFMR from C08b. A theoretical IFMR by Renedo et al. (2010; R10 hereafter) is shown as a dashed line. The empirical IFMR from our wide binary sample is shown as a dash-dot-dot line:

$$M_f = (0.452 \pm 0.045) + (0.073 \pm 0.019)M_i \quad (5)$$

The above relation excludes WD2253-08, the point in Fig. 6 at the upper left. We believe this is an outlier because of its low metallicity, as argued below.

Our IFMR can be adequately represented by a linear function (Equation 5) over the initial mass range $1.1 M_{\odot}$ to $4.1 M_{\odot}$. In general, it is similar to other empirical and theoretical relations. However, for higher M_i , the M_f from our IFMR is somewhat lower than other empirical relations. This is probably because only one WD has $M_i > 3 M_{\odot}$ in our sample. Like previous IFMR, the scatter in our relation is also larger than the formal error bars. This suggests other factors may affect the relation. Since the MS component to WD2253-08 has very low metallicity and is the biggest outlier in the relation shown in Fig. 6, we decided to test the influence of metallicity on the IFMR.

Fig. 7 shows lost mass fraction vs. $[\text{Fe}/\text{H}]$. Here $[\text{Fe}/\text{H}]$ is the original metallicity of the WD, as derived from its MS component’s spectrum. Two open circles represent DB

WDs. Three triangles are DA WDs whose initial masses were larger than $2 M_{\odot}$. The other five are DA WDs whose initial masses were lower than $2.0 M_{\odot}$. The dotted line is a least squares fit for these five DA WDs. There is a clear trend that suggests for a given initial mass, metal rich progenitors lose more mass when they evolve into WDs. We conclude that metallicity plays an important role in the amount of mass lost during post-MS evolution. In addition, the two DBs are both below the dashed line, tentatively suggesting that the metallicity dependence of post-MS mass loss may be different for DB than the DA stars.

6. Comparison between observations and theoretical models

Models suggest that the dependence of mass loss rates on stellar parameters is likely steep: along an evolutionary track $R(L, M, Z, \text{mixing length})$, the slope $d\log\dot{M}/d\log L$ from models ranges from ~ 3 for the Wachter et al. (2002) grid carbon-star models to > 16 for some of our model grids. For such large slopes, the star evolves at essentially constant mass to the death-zone, and leaves the death-zone along an essentially constant core mass track. The resulting IFMR is very close to what is found by taking the final mass to be the core mass at the death line, $M_{\text{final}} = L_{\text{Death}}(M_{\text{initial}})$. Note that M_{initial} here is the initial asymptotic giant branch (AGB) mass which may be smaller than the initial MS mass if significant mass loss occurs before the star reaches the AGB tip. It is known that low-mass, low- Z stars do lose significant mass before they leave the red giant branch (RGB), but we don't know how much mass is lost at that stage by stars with masses significantly greater than $1 M_{\odot}$.

Our model grids were computed with the Bowen code, using the following parameter values for our standard or “core” grid: the critical density for onset of density-dependent, less efficient, cooling is 10^{-12} gm/cm^3 ; the mean opacity for the atmosphere is $\langle \kappa_{\text{Rosseland}} \rangle = 0.0004 \text{ cm}^2/\text{gm}$; the dust condensation temperature is 1350 K with a condensation width $\Delta T = 100$; and the driving piston at the base of the model is constrained to an amplitude such that the maximum power does not exceed the stellar luminosity. See Willson (2000) and Willson & Wang (2011) for details.

In our grids, a model series for fixed M and Z assigned a radius to each L along the AGB track according to the following prescription:

$$R = 312(L/10^4)^{0.68}(1.175/M)^{0.31S}(Z/0.001)^{0.088}/(1/H)^{0.52} \quad (6)$$

where $S = 0$ for $M < 1.175$ and 1 for $M > 1.175 M_{\odot}$ and $1/H$ is the ratio of Iben

mixing length to scale height (Iben 1984). We have used the Iben mixing length ratio $l/H = 0.9$ which gives radii very close to standard evolutionary grids such as the Padova models (Girardi et al. 2000). A model series would describe the evolution of a single star if it were not for the evolving mass resulting from mass loss; we made model series to study the behavior of the mass loss law.

Metallicity dependence of the mass loss rate can come from two factors: (a) lower metallicity stars have smaller radii at a given L and M ; and (b) lower metallicity stars have a smaller maximum dust/gas ratio which helps expel material. For $d\log R/d\log Z = 0.088$ (Iben 1984) and $d\log \dot{M}/d\log R \sim 10$ (our models) we expect $d\log \dot{M}/d\log Z \sim 0.9$. This translates into $d\log L_{\text{death}}/d\log Z \sim 0.1$ for typical values of $d\log \dot{M}/d\log R$ and $d\log \dot{M}/d\log L$. The final mass is approximately $M_{\text{core}}(L_{\text{Death}}(M_{\text{iAGB}}))$ allowing us to link M_i to M_f via L_{death} .

Fig. 8 shows the agreement between our observations and two model grids. Model A (left panel) is our “core” case Bowen model described above, with no mass loss prior to the AGB. Varying model parameters (critical density for cooling, opacity, dust condensation temperature, or mixing length) has a small effect on the position of the $\Delta M/M_i$ vs Z points and almost no effect on the slope. However, it is known that at least some stars lose mass on the RGB. Model B (right panel) assumes that only low-mass stars lose appreciable mass on the RGB: $\Delta M_{\text{RGB}} = (2 - M_i) * 0.15$ for $1 M_{\odot} < M_i < 2 M_{\odot}$. We computed the standard deviation of the residuals, $\sqrt{\sum(\Delta M_{\text{observed}} - \Delta M)^2/5} = \text{SD5}$ for the 5 stars and the standard deviation for the four stars with the smallest error bars (SD4). Including RGB mass loss by the above prescription improves the fit slightly for the 5-star comparison and substantially for the 4-star comparison.

As stars evolve up the AGB, some have their envelopes enriched in carbon. As C/O rises, the radius for a given L , M , Z increases, and this will in turn enhance the mass loss rate at a given L (or core mass) and decrease the deathline L for a given M , Z . Using Figure 19 of Marigo & Girardi (2007) as a guide, we find that of the stars in our sample, only the one with initial mass = 2.9 solar masses is likely to have been a carbon star. However, the star with the lowest metallicity is close to the line dividing stars that do from stars that don’t, and any enhancement, even if C/O remains < 1 , will increase the radius and decrease the deathline L .

Overall, the mass loss models predict net mass loss and M_f vs. M_i that are very close to the values found from the WD+MS pairs. This will be true for other mass loss formulae with similar death-lines, as discussed by Willson (2007, 2008, 2009) and Willson et al. (2008). In addition, the Z -dependence of our models is consistent with the data from these WD+MS pairs. It is important to note that the bulk of the Z -dependence in the mass loss rates comes from the dependence of R on Z , with a smaller effect from the efficiency of forming dust (the

gas/dust ratio) in the models. Also, if C/O is increased over solar values this will decrease the final mass for a given initial mass and metallicity.

7. Conclusion

In this study, we constructed an empirical IFMR using 10 WDs in wide binaries. Our IFMR contains six WDs whose M_i are lower than $2 M_\odot$. They contribute to the low initial mass limit that is not well-sampled by clusters. Our WDs in wide binaries suggest a linear IFMR over the initial mass range $1.1 M_\odot$ to $4.1 M_\odot$ (Equation 5).

We compared our mass loss vs. metallicity relation to theoretical models for evolving lower MS stars ($< 2 M_\odot$). In general, the models predict a net mass loss and IFMR that agree with the values found from our observation within the current uncertainty of measurement.

Kalirai et al. (2007) and Kalirai et al. (2009) tentatively found a metallicity dependence on the IFMR. We find that at least part of the scatter seen in the IFMR is correlated with metallicity. Stars with lower metallicity apparently shed less mass when they become WDs.

Many thanks to D. Koester for providing his WD models. Balmer/Lyman lines in the models were calculated with the modified Stark broadening profiles of Tremblay & Bergeron, ApJ 696, 1755, 2009, kindly made available by the authors. T.D.O. acknowledges support from NSF grant AST-0807919 to Florida Institute of Technology. J.K.Z. and G.Z. acknowledge support from NSFC grant Nos. 11078019 and 10821061. L.A.W. and Q.W. acknowledge support from NSF grant AST-0708143.

REFERENCES

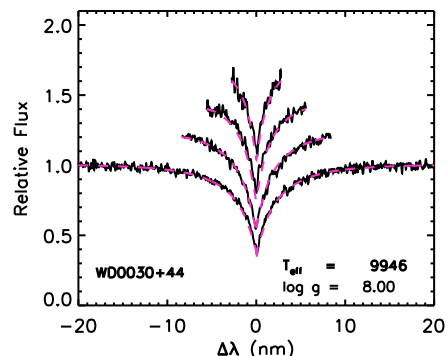
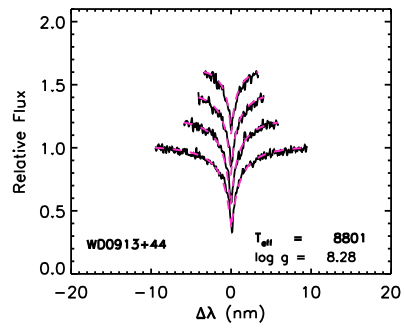
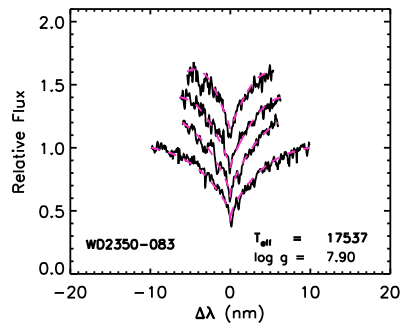
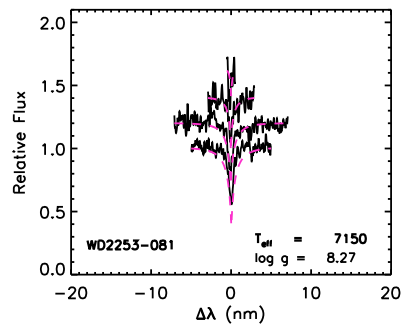
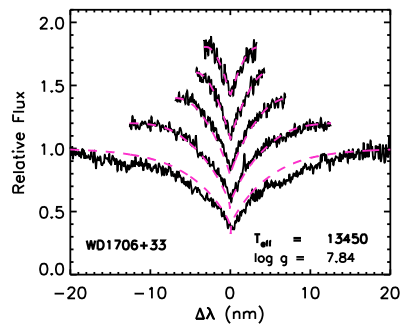
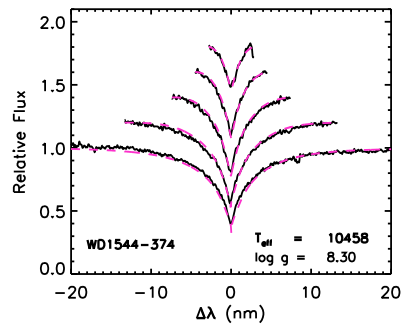
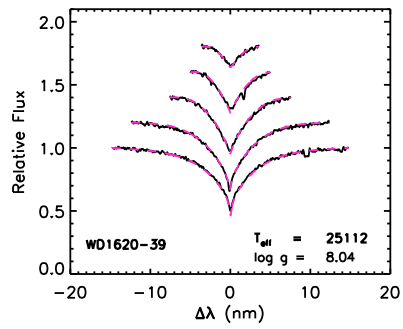
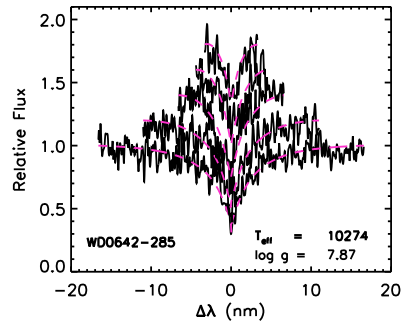
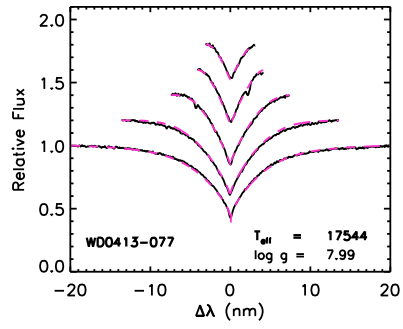
- Baliunas, S. L., et al. 1995, ApJ, 438, 269
- Barnes, S. A. 2007, ApJ, 669, 1167
- Bergeron, P., Saffer, R. A., & Liebert, J. 1992, ApJ, 394, 228
- Bergeron, P., Liebert, J., & Fulbright, M. S. 1995, ApJ, 444, 810
- Bergeron, P., Leggett, S. K., & Ruiz, M. T. 2001, ApJS, 133, 413
- Bochanski, J. J., West, A. A., Hawley, S. L., & Covey, K. R. 2007, AJ, 133, 531

- Castelli, F., Kurucz, R. L. 2003, in IAU Symp. 210, Modelling of Stellar Atmospheres, Poster Contributions, ed. N. Piskunov, W. W. Weiss, & D. F. Gray (San Francisco, CA: ASP), A20
- Catalán, S., Isern, J., García-Berro, E., Ribas, I., Allende Prieto, C., & Bonanos, A. Z. 2008a, A&A, 477, 213
- Catalán, S., Isern, J., García-Berro, E., & Ribas, I. 2008b, MNRAS, 387, 1693
- Claver, C. F., Liebert, J., Bergeron, P., & Koester, D. 2001, ApJ, 563, 987
- Donahue, R. A. 1993, Ph.D. Thesis, New Mexico State Univ. . 1998, ASP Conf Ser. 154, The Tenth Cambridge Workshop on Cool Stars, Stellar Systems and the Sun, ed. R. A. Donahue & J. A. Bookbinder(San Francisco: ASP), 1235
- Dobbie, P. D., et al. 2006, MNRAS, 369, 383
- Ferrario, L., Wickramainghe, D., Liebert, J., & Williams, K. A. 2005, MNRAS, 361, 1131
- Fontaine, G., Brassard, P., & Bergeron, P. 2001, PASP, 113, 409
- Genova, F. 2006, Centre de Données astronomiques de Strasbourg
<<http://simbad.u-strasbg.fr/>>
- Giampapa M. S., Hall G. C., Radick R. R., Baliunas S. L., 2006, ApJ, 651, 44
- Giclas, H. L., Burnham, R., & Thomas, N. G. 1971, Lowell Proper Motion Survey, Northern Hemisphere: The G Numbered Stars (Flagstaff: LowellObs.)
- Girardi, L., Bressan, A., Bertelli, G., & Chiosi, C. 2000, A&AS, 141, 371
- Hall, J. C., Lockwood, G. W., & Skiff, B. A. 2007, AJ, 133, 862
- Holmberg, J., Nordström, B., & Andersen, J., 2009, A&A, 501, 941
- Henry, T. J., Soderblom, D. R., Donahue, R. A., & Baliunas, S. L. 1996, AJ, 111, 439
- Iben, I., Jr. 1984, ApJ, 277, 333
- Jenkins, J. S. et al. 2011, A&A, 531, 8
- Kawka, A., Vennes, S., Schmidt, G. D., Wickramasinghe, D. T., & Koch, R. 2007, ApJ, 654, 499

- Kalirai, J. S., Richer, H. B., Reitzel, D., Hansen, B. M. S., Rich, R. M., Fahlman, G. G., Gibson, B. K., & von Hippel, T. 2005, *ApJ*, 618, L123
- Kalirai, J. S., Bergeron, P., Hansen, B. M. S., Kelson, D. D., Reitzel, D. B., Rich, R. M., & Richer, H. B. 2007, *ApJ*, 671, 748
- Kalirai, J. S., Hansen, B. M. S., Kelson, D. D., Reitzel, D., Rich, R. M., & Richer, H. B. 2008, *ApJ*, 676, 594
- Kalirai, J. S., Davis, D. S., Richer, H. B., Bergeron, P., Catelan, M., Hansen, B. M. S., & Rich, R. M. 2009, *ApJ*, 705, 408
- Koester, D., & Reimers D. 1996, *A&A*, 313, 810
- Koester, D., 2010, to appear in *Mem.S.A.I.*, based on lectures given at the School of Astrophysics "F. Lucchin", Tarquinia, June 2008 eprint arXiv:0812.0482
- Koester, D., Napiwotzki, R., Christlieb, N., Drechsel, H., Hagen, H. J., Heber, U., Homeier, D., & Karl, C. 2001, *A&A*, 378, 556
- Koester, D., Voss, B., Napiwotzki, R., Christlieb, N., Homeier, D., Lisker, T., Reimers, D., & Heber, U. 2009, *A&A*, 505, 441
- Lachaume, R., Dominik C., Lanz, T., & Habing H. J. 1999, *A&A*, 348, 897
- Luyten, W. J. 1979, *Proper Motion Survey with the 48 Inch Telescope* (Minneapolis: Univ. Minnesota Press)
- Mamajek, E. E., & Hillenbrand, L. A. 2008, *ApJ*, 687, 1264
- Marigo, P., & Girardi, L. 2007, *A&A*, 469, 239
- Markwardt, C. B., 2008, "Non-Linear Least Squares Fitting in IDL with MPFIT," in *proc. Astronomical Data Analysis Software and Systems XVIII*, Quebec, Canada, ASP Conference Series, Vol. 411, eds. D. Bohlender, P. Dowler & D. Durand (Astronomical Society of the Pacific: San Francisco), p. 251-254 (ISBN: 978-1-58381-702-5; ADS Bibcode: 2009ASPC..411..251M (click for Bibtex and other citation formats) Arxiv preprint: arXiv:0902.2850v1
- Noyes, R. W., Hartmann, L. W., Baliunas, S. L., Duncan, D. K., & Vaughan, A. H. 1984, *ApJ*, 279, 763
- Oswalt, T. D., Hintzen, P. M., & Luyten, W. J. 1988, *ApJS*, 66, 3910

- Oswalt, T. D., Smith, J. A., Shufelt, S., Hintzen, P. M., Leggett, S. K., Liebert, J., & Sion, E. M. 1993, in *White Dwarfs: Advances in Observation and Theory*, ed. M. A. Barstow (NATO ASI Ser. C, 403; Dordrecht: Kluwer), 419
- Reid, I. N. 1996, *AJ*, 111, 2000
- Reimers, D., & Koester, D. 1982, *A&A*, 116, 341
- Renedo, I., Althaus, L. G., Miller Bertolami, M. M., Romero, A. D., Córscico, A. H., Rohrmann, R. D., & García-Berro, E. 2010, *ApJ*, 717, 183
- Rocha-Pinto, H. J., & Maciel, W. J. 1998, *MNRAS*, 298, 332
- Rocha-Pinto, H. J., Maciel, W. J., Scalo, J., & Flynn, C. 2000, *MNRAS*, 358, 850
- Rubin, K. H. R., Williams, K. A., Bolte, M., & Koester, D. 2008, *AJ*, 135, 2163
- Silvestri, N. M., Oswalt, T. D., Wood, M. A., Smith, A. J., Reid, I. N., & Sion, E. M. 2001, *AJ*, 121, 503
- Silvestri, N. M., Oswalt, T. D., & Hawley, S. L. 2002, *AJ*, 124, 1118
- Silvestri, N. M., Hawley, S. L., & Oswalt, T. D. 2005, *AJ*, 129, 2428
- Skumanich, A. 1972, *ApJ*, 171, 565
- Smith, J. A. 1997, Ph.D. Dissertation, Florida Institute of Technology
- Soderblom, D. R., Duncan, D. K., & Johnson, D. H. R. 1991, *ApJ*, 375, 722
- Soderblom, D. R., 2010, *Annu. Rev. Astron. Astrophys.*, 48, 581
- Valenti J. A., Fischer D. A., 2005, *ApJS*, 159, 141
- Vaughan, A. H., & Preston, G. W. 1980, *PASP*, 92, 385
- Vauclair, G., Schmidt, H., Koester, D., & Allard, N. 1997, *A&A*, 325, 1055
- Voss, B., Koester, D., Napiwotzki, R., Christlieb, N., & Reimers, D. 2007, *A&A*, 470, 1079
- Wachter, A., Schröder, K. -P., Winters, J. M., Arndt, T. U., & Sedlmayr, E. 2002, *A&A*, 384, 452
- Weidemann, V. 1977, *A&A*, 59, 418
- Weidemann, V. 2000, *A&A*, 363, 647

- Williams, K. A., Bolte, M., & Koester, D. 2004, *ApJ*, 615, L49
- Williams, K. A., 15th European Workshop on White Dwarfs ASP Conference Series, Vol. 372, proceedings of the conference held 7-11 August, 2006 in Leicester, United Kingdom. Edited by Ralf Napiwotzki and Matthew R. Burleigh. San Francisco: Astronomical Society of the Pacific, 2007., p.85
- Williams, K. A., Bolte, M., & Koester, D. 2009, *ApJ*, 693, 355
- Wilson, O. C. 1963, *ApJ*, 138, 832
- Wilson, O. C. 1968, *ApJ*, 153, 221
- Willson, L. A. 2000, *ARA&A*, 38, 573
- Willson, L. A. 2007, Why Galaxies Care About AGB Stars: Their Importance as Actors and Probes. ASP Conference Series, Vol. 378, proceedings of the conference held 7-11 August 2006 at University Campus, Vienna, Austria. Edited by F. Kerschbaum, C. Charbonnel, and R. F. Wing. San Francisco: Astronomical Society of the Pacific, 2007., p.211
- Willson, L. A. 2008, The Art of Modeling Stars in the 21st Century, Proceedings of the International Astronomical Union, IAU Symposium, Volume 252, p. 189-195
- Willson, L. A., Struck, C., Wang, Q., & Kawaler, S. D. 2008, *Physica Scripta*, Volume 133, Issue , pp. 014008 (2008).
- Willson, L. A. 2009, The Biggest, Baddest, Coolest Stars ASP Conference Series, Vol. 412, proceedings of the workshop held 16-18 July 2007, at the Millennium Centre, Johnson City, Tennessee, USA. Edited by Donald G. Luttermoser, Beverly J. Smith, and Robert E. Stencel. San Francisco: Astronomical Society of the Pacific, 2009., p.137
- Willson, L. A., & Wang, Q. 2011, in prep
- Wood, M. 1995, *White Dwarfs*, ed. D. Koester & K. Werner, vol. 443, (Berlin: Springer), 41
- Zhao, J. K., Oswalt, T. D., Rudkin, M., Zhao, G., & Chen, Y. Q. 2011a, *AJ*, 141, 107
- Zhao, J. K., Zhao, G., Chen, Y. Q., & Luo, A. L. 2011b, *Research in Astronomy and Astrophysics*, 11, 563



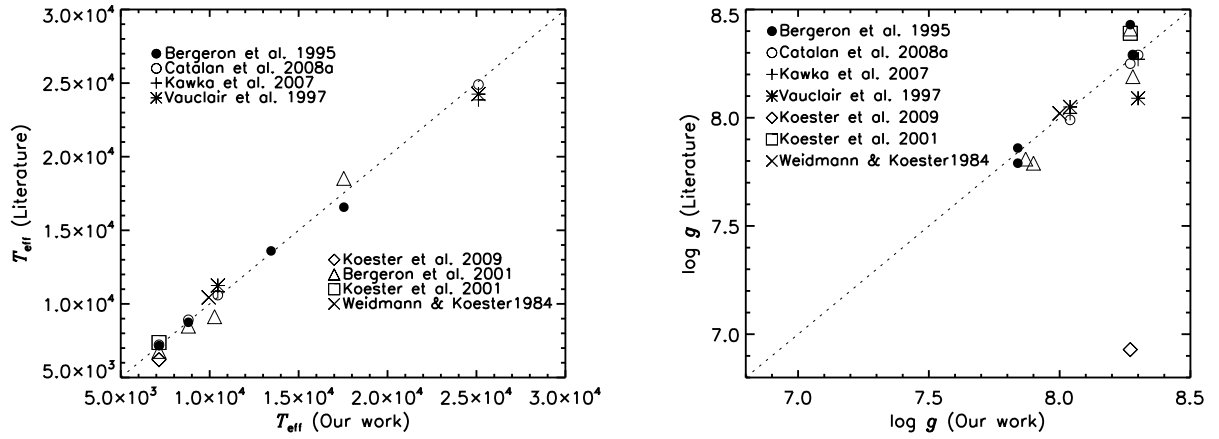
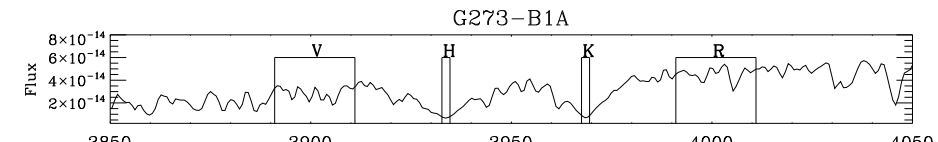
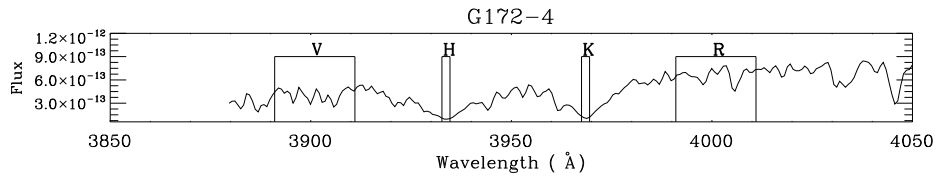
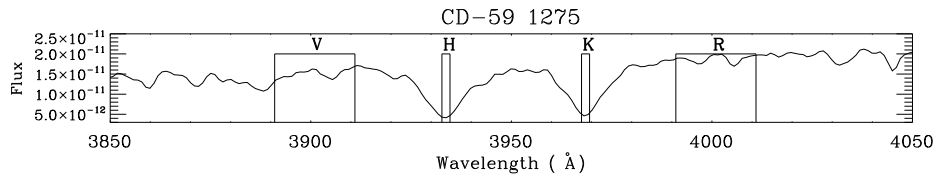
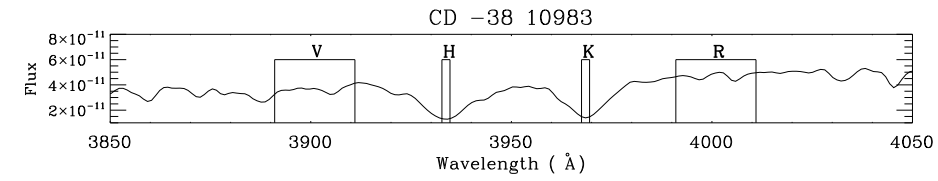
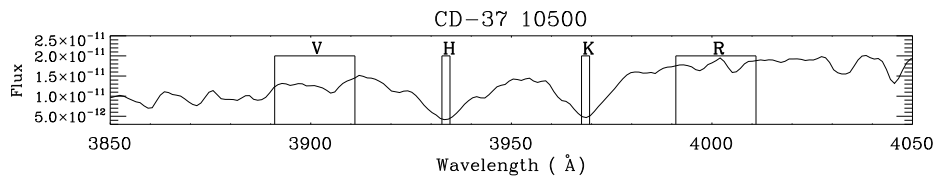
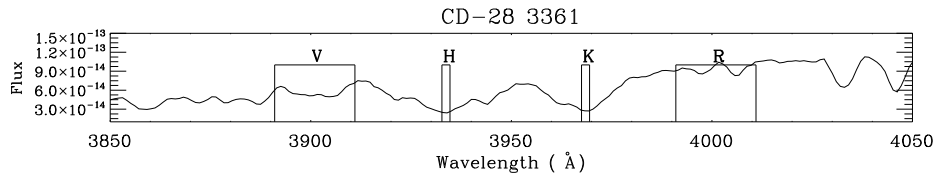
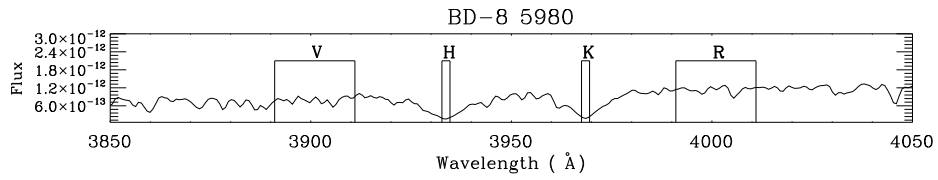
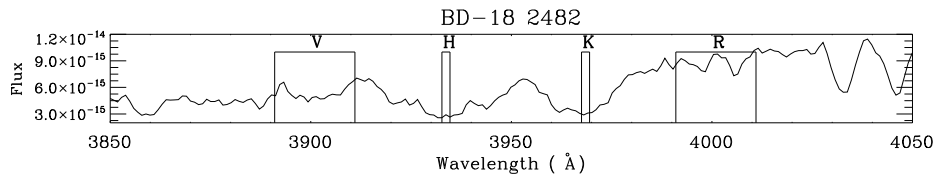
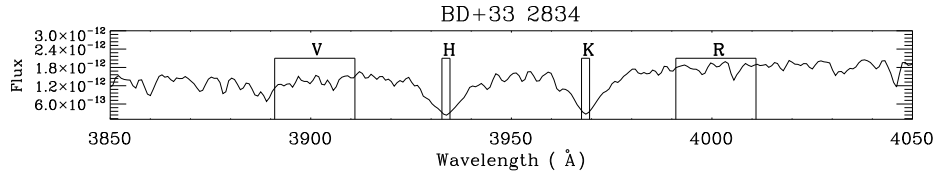
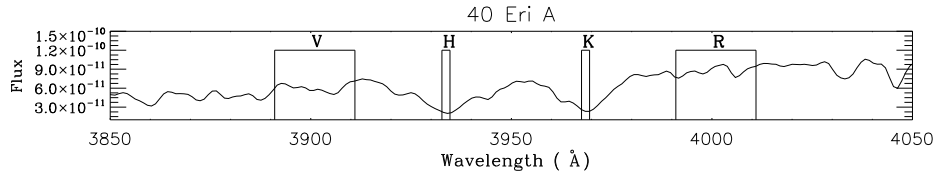


Fig. 2.— T_{eff} and $\log g$ comparison between our results and those from the literature. The dotted line is the unit slope relation.



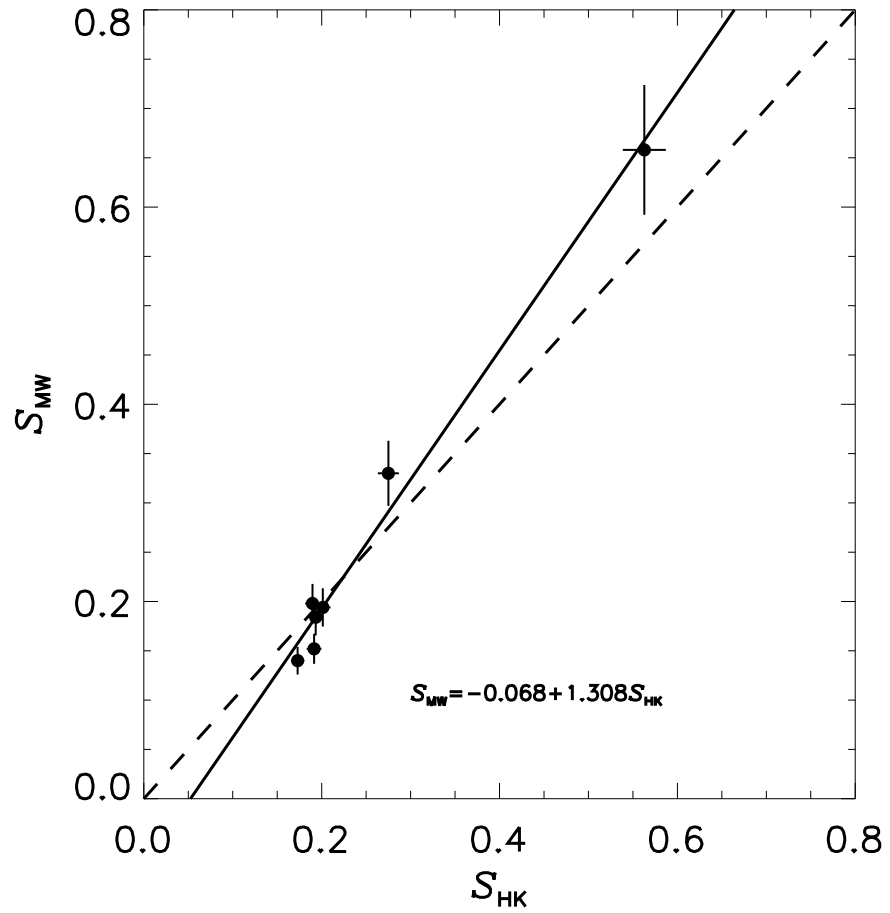


Fig. 4.— Calibration between our chromospheric activity index S_{HK} and the Mount Wilson S_{MW} index. The solid line is the least squares fit, while a dashed line is the unit slope relation.

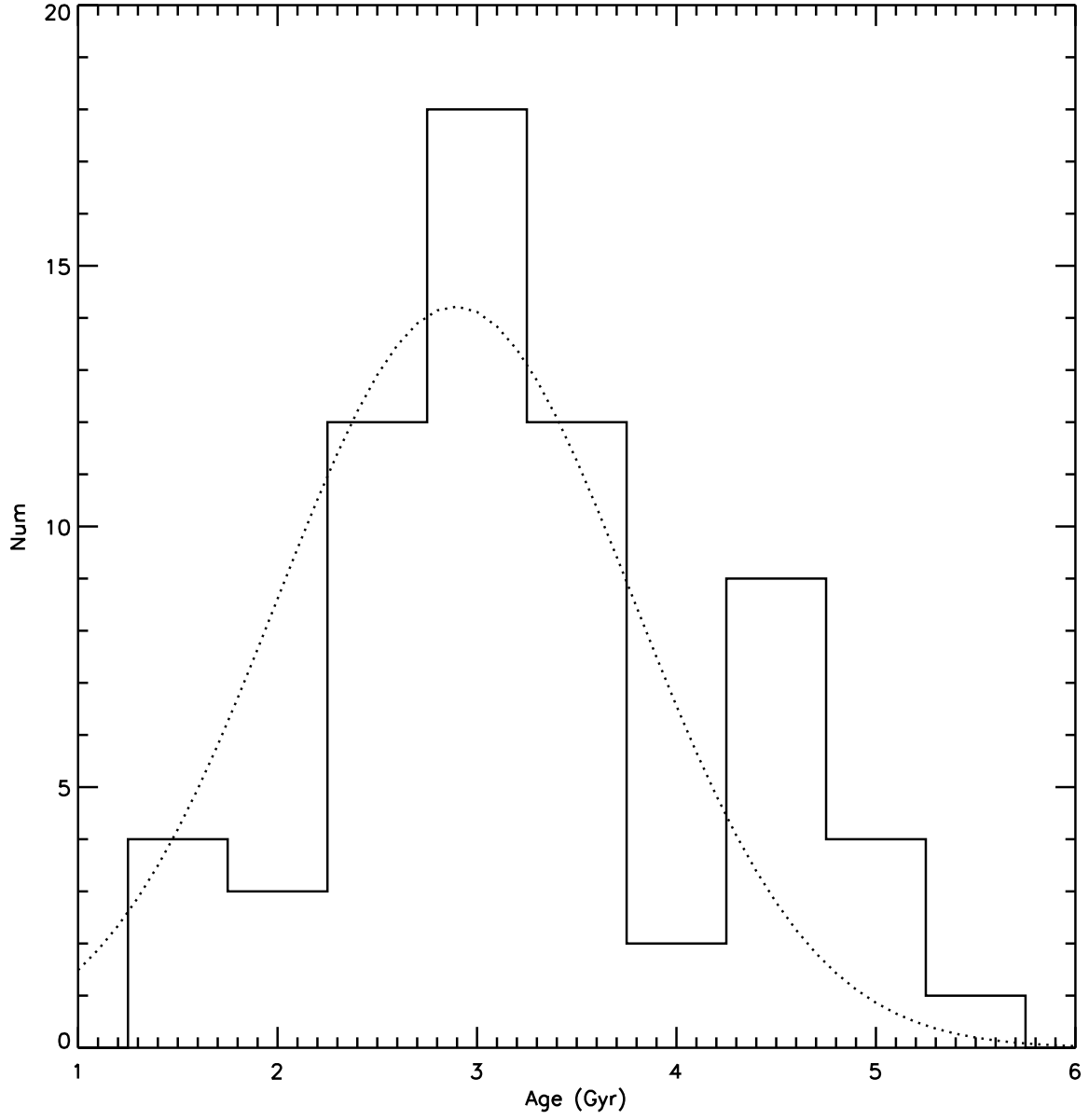


Fig. 5.— The chromospheric activity distribution of M67 member stars. The dotted line is the Gaussian fitting.

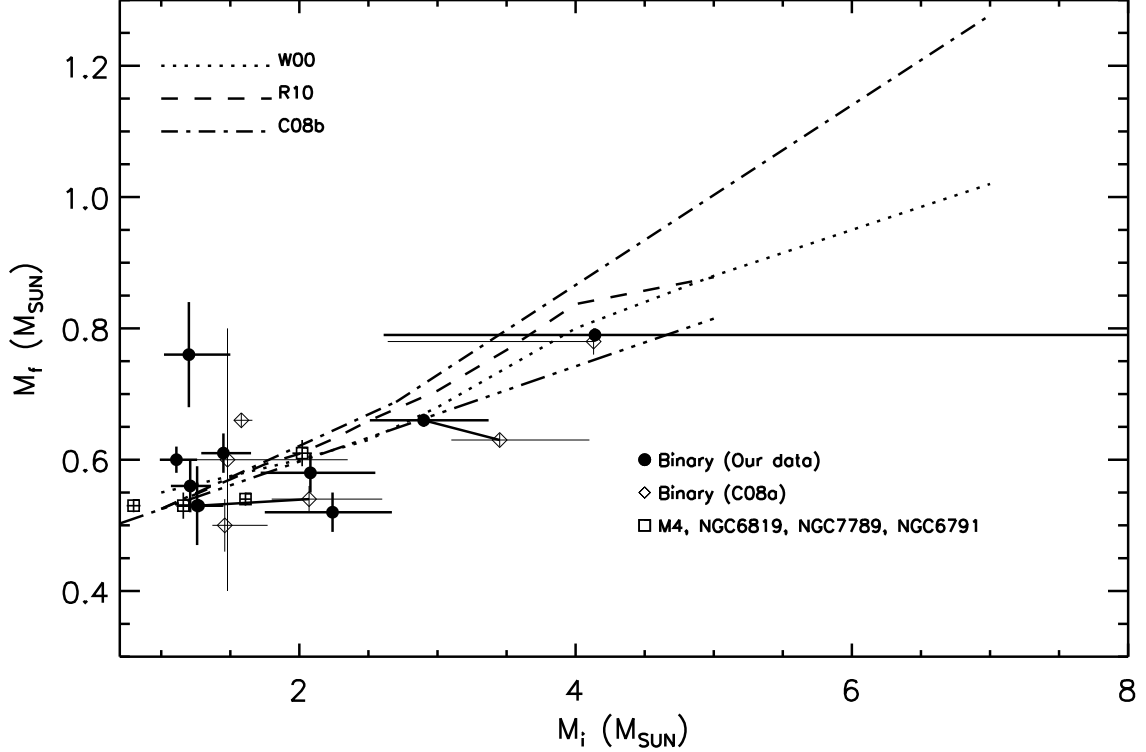


Fig. 6.— WD initial-final mass relationship shown for the 10 WDs in this work (filled circles). The Diamonds represent the WDs in wide binaries from Catalán et al. (2008a). The dotted line is the empirical IFMR of Weidemann (2000). The dashed line is the theoretical IFMR ($Z = 0.01$) from Renedo et al. (2010). The dashed dot line is the empirical IFMR from Catalán et al. (2008b). The dash-dot-dot line is a least squares fit of 9 WDs (not including the left top star WD2253-08) in our paper. The solid lines connect the WD points both in our paper and Catalán et al. (2008a). The squares represent mean M_f and M_i values of WDs in four clusters: M4, NGC6819, NGC7789 and NGC6791.

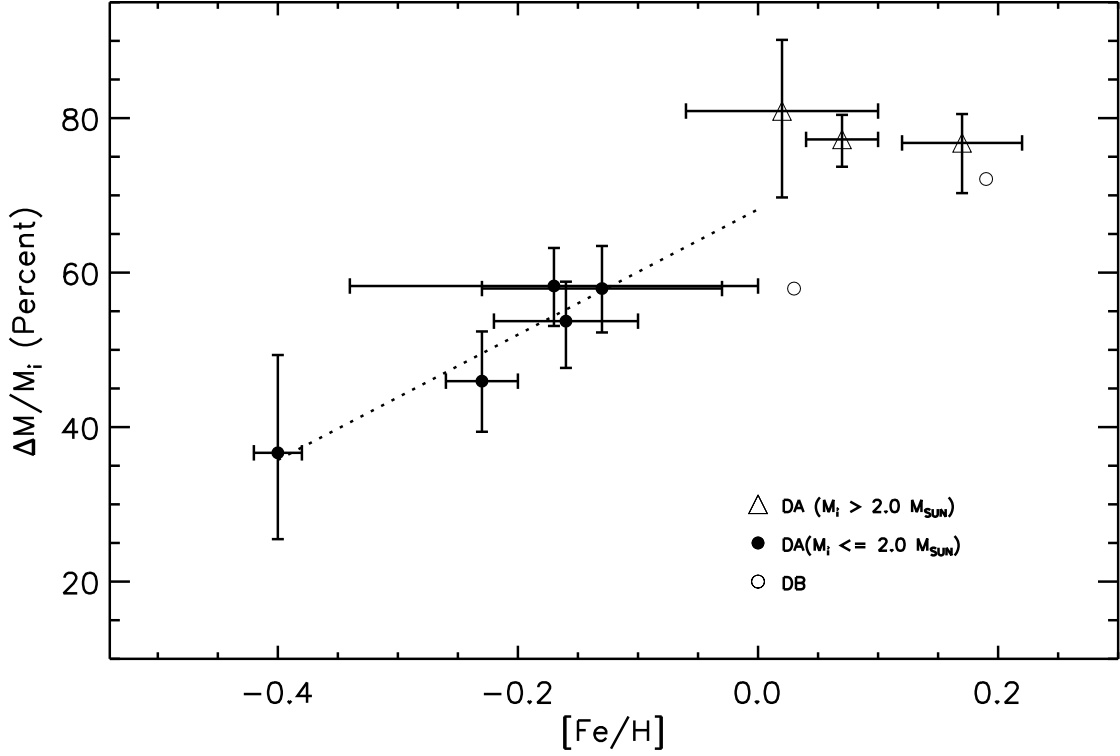


Fig. 7.— Lost mass fraction vs. $[\text{Fe}/\text{H}]$. Triangles are WDs with $M_i > 2.0 M_\odot$. Filled circles are DA WDs and open circles are DB WDs. Dotted line is the fit from 5 DA WDs with M_i smaller than $2.0 M_\odot$.

Table 1. Wide binaries in our sample

Wide Binary (1)	RA (2)	Dec (3)	White Dwarf (4)	Spectral Type (5)	UT (6)	Site (7)
40 Eri A/B	04 13 03	-07 44 06	WD0413-077	DA	02/04	CTIO
CD-59 1275/L182 61	06 15 36	-59 11 24	WD0615-591	DB	02/04	CTIO
CD-28 3361/LP895-41	06 42 34	-28 30 48	WD0642-28	DA	02/04	CTIO
BD-18 2482/LP786-6	08 45 18	-18 48 00	WD0845-188	DB	02/04	CTIO
CD-38 10983/10980	16 20 38	-39 04 42	WD1620-39	DA	02/04	CTIO
CD-37 10500/L481-60	15 44 12	-37 46 00	WD1544-374	DA	02/04	CTIO
BD+33 2834/G181-B5B	17 06 58	33 16 48	WD1706+33	DA	07/10	KPNO
BD-8 5980/G156-64	22 53 12	-08 05 24	WD2253-08	DA	07/10	KPNO
G273-B1A/B	23 50 54	-08 21 06	WD2350-083	DA	11/06	KPNO
BD+44 1847/G116-16 ^a	09 11 51	44 15 36	WD0913+44	DA	11/06	KPNO
G172-4/G171-62	00 30 17	44 27 18	WD0030+44	DA	11/06	KPNO

^aNon-physical pair; see text.

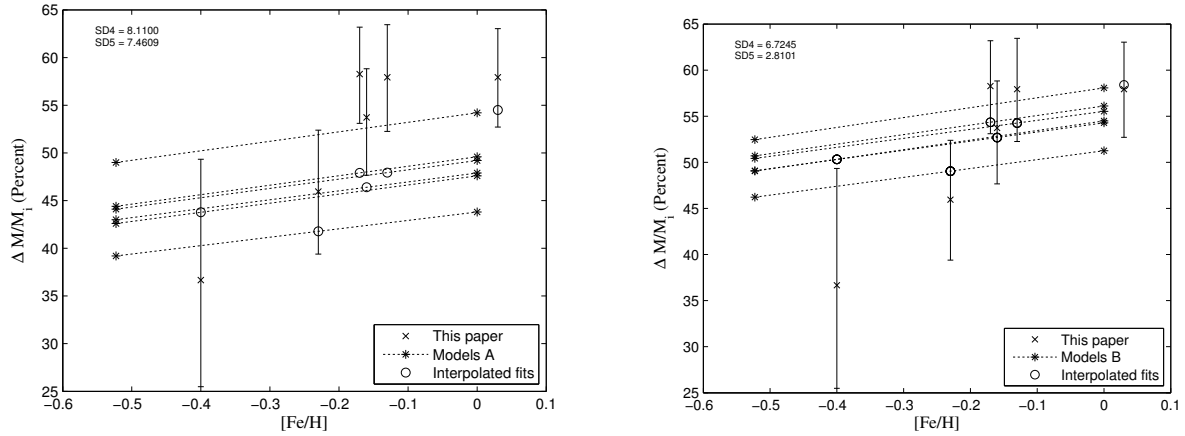


Fig. 8.— Comparison of observed lost mass fraction from Figure 6 with two model sets. In each graph, the points marked by asterisks are derived as described in the text from a series of models with the same masses as the observed stars but with two different values for Z . The fits for each of the observed stars (open circles) are then obtained by interpolating between the two Z model sets along a fixed-mass (dashed) line. Case A is our standard “core” model as described in the text. To test the effects of mass loss by low mass stars ($< 2 M_{\odot}$) along the RGB or at the core flash, we also computed case B with a prescription for RGB mass loss given by $\Delta M_{\text{RGB}} = 0.15 (2 - M_{\text{initial}})$ for $1 < M_{\text{initial}} < 2$. This was chosen as the simplest rule giving reasonable ΔM_{RGB} for $M = 1$ and $M = 2$. SD5 and SD4 are the standard deviations of the residuals including 5 and 4 stars (the latter omitted the one with the largest error bars).

Table 2. Physical properties of WDs in wide binaries

Name	S/N ^a	T_{eff}	$\log g$	M_f	t_{cool}	$t_{\text{progenitor}}$	[Fe/H]	M_i
(1)	(2)	(3)	(4)	(5)	(6)	(7)	(8)	
WD0413-077	240	17544±64	7.84±0.01	0.53±0.01	0.086±0.028	3.48 ^{5.19} _{2.33}	-0.17±0.17	1.27 ^{1.44} _{1.13}
WD0642-28	57	10274±122	7.87±0.12	0.53±0.06	0.482±0.077	3.67 ^{5.66} _{2.32}	-0.13±0.10	1.26 ^{1.45} _{1.11}
WD1620-39	156	25112±102	8.04±0.01	0.66±0.01	0.025±0.001	0.52 ^{0.79} _{0.35}	0.07±0.03	2.90 ^{2.51} _{3.37}
WD1544-374	242	10458±25	8.30±0.02	0.79±0.01	0.844±0.025	0.20 ^{0.70} _{0.01}	0.02±0.08	4.14 ^{8.00} _{2.61}
WD1706+33	34	13450±453	7.84±0.05	0.52±0.03	0.219±0.038	1.08 ^{1.71} _{0.66}	0.17±0.05	2.24 ^{2.67} _{1.75}
WD2253-08	45	7150±67	8.27±0.12	0.76±0.08	2.470±0.739	4.07 ^{7.20} _{1.95}	-0.40±0.02	1.20 ^{1.50} _{1.02}
WD2350-083	52	17537±266	7.90±0.07	0.56±0.04	0.097±0.015	4.18 ^{6.28} _{2.79}	-0.16±0.06	1.21 ^{1.36} _{1.07}
WD0030+44	46	9946±34	8.00±0.04	0.60±0.02	0.612±0.041	5.38 ^{8.25} _{3.44}	-0.23±0.03	1.11 ^{1.26} _{0.99}
WD0615-591 ^b	<20	16714±200	8.02±0.05	0.61±0.03	0.155±0.016	3.01 ^{4.53} _{1.99}	0.03±0.07	1.45 ^{1.65} _{1.29}
WD0845-188 ^b	<20	17566±350	7.97±0.05	0.58±0.03	0.118±0.013	1.18 ^{1.80} _{0.76}	0.19±0.09	2.08 ^{2.55} _{1.72}

^aAverage S/N surrounding H δ .

^bThe type of WD is DB. T_{eff} and $\log g$ are from Voss et al. (2007).

Table 3. CA standard stars

Name	B-V	S_{HK}	S_{MW}
(1)	(2)	(3)	(4)
HD212754	0.520	0.173	0.140
HD206860	0.590	0.275	0.330
HD207978	0.420	0.192	0.152
HD224930	0.670	0.193	0.184
HD10476	0.840	0.190	0.198
HD190406	0.610	0.201	0.194

Table 4. Ages of the wide binaries estimated by CA

Name	B-V	S_{HK}	S_{MW}	R'_{HK}	age
(1)	(2)	(3)	(4)	(5)	(6)
40 Eri A/B	0.775	0.305	0.206	-4.85	3.56 ^{5.28} _{2.41}
CD-59 1275/L182-61	0.590	0.268	0.156	-4.99	3.17 ^{4.68} _{2.14}
CD-28 3361/LP895-41	0.972	0.346	0.238	-4.92	4.15 ^{6.14} _{2.81}
BD-18 2482/LP786	1.036	0.407	0.307	-4.88	1.29 ^{1.91} _{0.87}
CD-38 10983/CD-38 10980	0.630	0.325	0.29	-4.52	0.55 ^{0.81} _{0.37}
CD-37 10500/L481-60	0.718	0.303	0.256	-4.66	1.05 ^{1.55} _{0.71}
BD+33 2834/G181-B5B	0.568	0.188	0.171	-4.87	1.30 ^{1.93} _{0.88}
BD-8 5980/G156-64	0.630	0.197	0.188	-4.84	6.54 ^{9.67} _{4.42}
G273-B1A/B	0.770	0.196	0.188	-4.91	4.28 ^{6.32} _{2.89}
G171-62/G172-4	0.980	0.230	0.232	-4.94	5.99 ^{8.86} _{4.05}

Table 5. Comparison between our ages and those from the literature

Name	age ^a (Gyr)	age ^b (Gyr)	rotation age ^c (Gyr)	our age (Gyr)
(1)	(2)	(3)	(4)	(5)
40 Eri A	~	12.2 ^{14.5} _{8.5}	4.75±0.75	3.56 ^{5.28} _{2.41}
CD-38 10983	2.5 ^{7.0} _~	2.0 ^{3.9} _{0.4}	0.58±0.08	0.55 ^{0.81} _{0.37}
CD-59 1275	5.9 ^{6.6} _{5.4}	3.7 ^{4.7} _{3.4}		3.17 ^{4.68} _{2.14}
CD-37 10500	7.4 ^{13.0} _{1.9}	4.4 ^{7.0} _{1.4}		1.05 ^{1.55} _{0.71}

^aages are from Holmberg, Nordström & Andersen (2009)

^bages are from Valenti & Fischer (2005)

^cages are from Barnes (2007)